Hindawi
Mathematical Problems in Engineering
Volume 2020, Article ID 7024740, 14 pages
https://doi.org/10.1155/2020/7024740

Research Article

Research on Transmission Efficiency Oriented Predictive Control of Power Split Hybrid Electric Vehicle

Hongdang Zhang,[1,2] Dehua Shi ,[1,3] Yingfeng Cai ,[3] Weiqi Zhou ,[3] and Hongtu Yang[1,2]

[1]*School of Automobile and Traffic Engineering, Jiangsu University, Zhenjiang 212013, China*
[2]*Changzhou Institute of Mechatronic Technology, Changzhou 213164, China*
[3]*Jiangsu Chunlan Clean Energy Research Institute Co., Ltd., Taizhou 225300, China*

Correspondence should be addressed to Dehua Shi; dhshi@ujs.edu.cn

Received 28 August 2019; Revised 22 November 2019; Accepted 4 February 2020; Published 17 March 2020

Academic Editor: Luis J. Yebra

Power split hybrid electric vehicle (HEV), which enables free adjustment of the engine, shows excellent performance in energy saving. The fuel economy of HEV is influenced by the battery charging/discharging. In order to maintain the exact battery sustainability, dynamic programming, a kind of global optimization strategy, is applied offline to derive the optimal solutions with minimal engine fuel consumption and exact battery SOC balance. The mode switching rules are further extracted and used to decide the operation modes for real-time control applications. The operation efficiencies of different components are analyzed, and the system transmission efficiency for the operation mode that both the engine and electric machines are engaged in is obtained. Then, the optimal problem based on model predictive control scheme is constructed with the objective of maximal powertrain transmission efficiency. The optimal problem in the prediction horizon is solved by dynamic programming to obtain the optimal control sequence. Finally, simulation studies are made. Simulation results demonstrate that the transmission efficiency oriented predictive strategy can maintain the battery charging sustainability and improve the equivalent fuel economy of the HEV effectively. The results validate the feasibility and superiority of the proposed controller.

1. Introduction

Hybrid electric vehicle (HEV) demonstrates good solutions in dealing with the environmental pollutions and oil crisis due to the added electric source. The HEV configurations are mainly categorized as parallel, series, and series-parallel type (usually power split configuration) [1, 2]. The series type HEV can reduce fuel consumption for low velocities by preventing the engine from operating at low efficiency regions. However, at high velocities, the energy losses of series type HEV increase because the mechanical output energy of the engine is converted in twice, and the engine prefers to drive the wheels directly. The parallel HEV, in contrast, shows good fuel economy for medium and high velocity scenarios with appropriate transmission ratio, but bad results at low velocities, because of the mechanical connection between the wheel and engine [3]. The series-parallel type HEV, also known as the power split ones, inherits the advantages of both series and parallel type HEVs. They are dominating the markets, such as Toyota Prius, Ford Fusion, Chevrolet Volt, and Buick Velite [4, 5].

The energy management strategy is the core to the powertrain in deciding the output power of different power sources, on which abundant research studies have been conducted. The strategies can be classified as rule-based and optimization-based types [1–3]. Although rule-based strategies demonstrate bad robustness which means that the mode switching rules predefined for certain driving cycles may behave badly for other scenarios, they are widely used in practical applications because of easy implementation and the advantages in real-time capability. Besides, the predefined rules can be independent of the driving cycle. By optimizing the rules for certain driving cycles with optimal algorithms, such as particle swarm optimization, genetic

algorithm, and so on, rule-based strategies can even gain near-optimal results [6, 7]. Optimization-based strategies are used to derive the global or instantaneous optimal solutions with different kinds of optimization algorithms. For example, dynamic programming, a kind of global optimization strategy, can be used to obtain the optimal control sequence by minimizing certain cost functions in the whole time history, while equivalent consumption minimization strategy (ECMS) and Pontryagin's minimal principle (PMP) deal with energy management at each moment and can be run in real time [8–10]. Model predictive control (MPC) makes full use of future information and solves the optimal problem in a finite time horizon. Therefore, MPC proves to be a good compromise between the global and instantaneous solutions [11, 12].

By reviewing the existing optimal energy management strategies, it can be found that most of them have focused on the minimization of engine fuel consumption, which often leads to the crude consideration of powertrain energy losses, such as the energy conversion losses that occur in the battery and electric machines [13]. Lowest energy consumption instead of engine fuel consumption can be maintained by maximizing the energy conversion efficiency [14]. The HEV powertrain efficiency has been studied in depth to reveal the energy flows and energy losses for different energy paths in some works [15–18]. Aiming at improving the operation efficiency of hybrid powertrain, Schouten et al. analyzed the component efficiency of a parallel HEV and derived the heuristic control rules [19]. Shabbir and Evangelou considered the efficiency of engine-generator set, the battery, and power electronics. On this basis, a control map was produced to ensure the maximum powertrain efficiency for a series HEV [13]. As for power split HEV, the planetary power coupling configuration has the mechanical point at which all the engine power flows to wheels and the battery power equals zero. According to this mechanical point, the engine speed can be decided for certain vehicle velocity to maintain high powertrain efficiency [20–22]. Wang et al. proposed the separation factor which is related to the engine and vehicle speed and further designed the instantaneous optimal strategy to improve the economical efficiency [23]. However, the mechanical point oriented strategy just focused on the vehicle speed and ignored the effects of engine torque on the transmission efficiency. The engine torque should also be accounted for the system efficiency.

This paper investigates the energy management strategy of a power split HEV based on optimal transmission efficiency when the engine is start up. When the engine is shut down, the vehicle is solely driven by the motor as pure electric driving. It is important to identify whether the engine should be started up or shut down during the driving process. Therefore, the laws that are beneficial to judge the engine operation states are extracted based on the global optimal results derived by dynamic programming (DP). In the operation mode that the engine works, the system transmission efficiency is derived based on the efficiencies of different components. Model predictive control which is capable of dealing with constrained optimal problems in finite time horizon is further applied to construct the energy distribution problem, and DP is implemented to derive the optimal engine operation point. The proposed transmission efficiency oriented predictive strategy (TEOPS) is benchmarked against the rule-based strategy and the ECMS which have shown the real-time capability and easy implementation.

The rest of the paper is presented as follows. The powertrain model is established in Section 2, followed by the analyses of powertrain transmission efficiency in Section 3. Section 4 gives the optimal energy management strategy. In Section 5, comparative simulations are conducted, and the conclusions are drawn in Section 6.

2. Modeling of the Powertrain

Figure 1 gives the configuration of the HEV powertrain, where the power coupling device with planetary gear sets (PG1 and PG2) is used to connect the engine and electric machines (MG1 and MG2). Electric machines are connected to the sun gears of PG1 and PG2. The engine is connected to the carrier gear of PG1. The carrier gear of PG2 is connected to the ring gear of PG1 and transmits the power to the final drive. By controlling the operation states of the engine and electric machines, the vehicle can realize different modes, including the charging while standstill, pure electric driving, hybrid driving, regenerative braking, and mechanical braking.

The dynamic equations of the planetary power coupling device can be derived based on lever analogy [24]. Since each planetary gear set has both translational and rotational degrees of freedom (DOF), four dynamic torque relations of the configuration are established. Due to the mechanical connections between different parts of the planetary gear sets, the system torque and speed constraints are obtained. Consequently, the powertrain dynamic relations with the engine speed ω_{E} and the rotational speed ω_{out} of the second carrier as state variables are described as

$$\begin{bmatrix} \dot{\omega}_{\mathrm{E}} \\ \dot{\omega}_{\mathrm{out}} \end{bmatrix} = \begin{bmatrix} I_{\mathrm{gt}}(1+K_1)^2 + I_{\mathrm{et}} & -I_{\mathrm{gt}}K_1(1+K_1) \\ I_{\mathrm{gt}}(1+K_1) + I_{\mathrm{et}} & -K_1 I_{\mathrm{gt}} + (1+K_1)^2 I_{\mathrm{mt}} + I_{\mathrm{outt}} \end{bmatrix} \cdot \begin{bmatrix} (1+K_1)T_{\mathrm{G}} + T_{\mathrm{E}} \\ (1+K_2)T_{\mathrm{M}} + T_{\mathrm{E}} + T_{\mathrm{G}} + T_{\mathrm{out}} \end{bmatrix}, \tag{1}$$

where K_1 and K_2 are the ratio between the radius of the ring gear and the sun gear for PG1 and PG2, respectively. T_{E} is the engine torque, while T_{G} and T_{M} denote the torque of MG1 and MG2, respectively. T_{out} is the load torque and is written as

$$T_{\mathrm{out}} = \frac{T_{\mathrm{brk}} + [mg(f\cos\theta + \sin\theta)]R_{\mathrm{w}}}{i_{\mathrm{d}}} + \frac{0.5\rho_{\mathrm{air}}A_f C_{\mathrm{d}}(\omega_{\mathrm{out}}/i_{\mathrm{d}})^2 R_{\mathrm{w}}^3}{i_{\mathrm{d}}}, \tag{2}$$

where T_{brk} is the friction torque; i_{d} is the ratio of final drive; θ is the road slope; m is the vehicle mass; f is the coefficient of

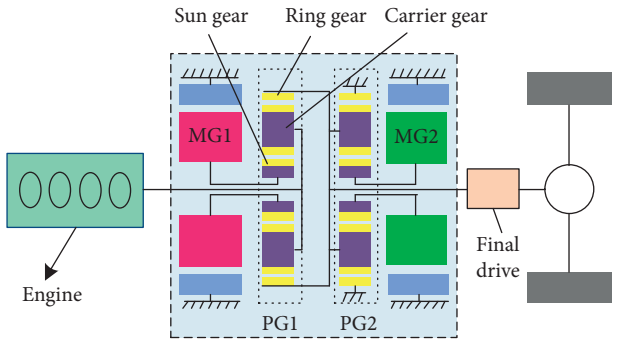

Figure 1: Configuration of the powertrain.

rolling resistance; A_f and C_d are the vehicle frontal area and air drag coefficient, respectively; ρ_{air} is the air density; and R_w is the inertia of the wheel.

I_{et}, I_{gt}, I_{mt}, and I_{outt} are lumped rotational inertias. They are given by

$$\begin{cases} I_{et} = I_E + I_{C1}, \\ I_{gt} = I_G + I_{S1}, \\ I_{mt} = I_G + I_{S2}, \\ I_{outt} = I_{R1} + I_{C2} + I_{fd} + \dfrac{(mR_w^2 + 4I_w)}{i_d^2}, \end{cases} \tag{3}$$

where I_G, I_E, and I_M are rotational inertias of different power sources; I_{C1}, I_{S1}, I_{C2}, and I_{S2} are rotational inertias of the planetary gears; and I_{fd} and I_w are the inertia of the final drive and the wheel.

The parameters of the power split HEV are shown in Table 1.

3. Analysis of the Operation Efficiency

The proposed power coupling device can act as an electric continuous variable transmission (ECVT) to regulate the engine torque and speed continuously, which is similar to the Toyota Prius. Therefore, the transmission which includes the hydraulic torque converter and clutch is removed from the powertrain. The other mechanical efficiency mainly lies in the final drive and the planetary gear set. Once the vehicle speed and acceleration are decided, the required torque and speed at the output shaft of the planetary gear set are also certain, leading to certain final drive efficiency. Therefore, the efficiency caused by the final drive has the same influence on different energy management strategies. Consequently, by referring to the modeling method in ADVISOR, constant efficiency of the final drive is applied, which is set to be 97%. It is pointed out that gear loss was assumed to be 1% of the transmitted torque used in the automotive industry [25]. For simplification of the controller design, the transmission efficiency of the planetary gear set is assumed to be 100%.

Table 1: Parameters of the powertrain.

Parameter	Value	Unit
Vehicle mass m	12980	kg
Wheel radius R_w	0.47	m
Air density ρ_{air}	1.23	g/m^3
Coefficient of rolling resistance f	0.0135	—
Ratio of the final drive i_d	4.875	—
Air drag coefficient C_d	0.65	—
Vehicle front area A_f	7.1	m^2
K_1, K_2	2.11, 2.11	—
Maximal engine speed ω_{max}^E	2500	r/min
Maximal engine torque T_{max}^E	650	Nm
Maximal speed of MG1 ω_{max}^G	5000	r/min
Maximal torque of MG1 T_{max}^G	400	Nm
Maximal speed of MG2 ω_{max}^M	7500	r/min
Maximal torque of MG2 T_{max}^M	700	Nm
Rate voltage of the battery U_{ocr}	530	V
Rate capacity of the battery Q_{batr}	70	Ah

3.1. Efficiency Model of Different Components. During braking process, the engine is shut down and the energy management strategy can be designed to fully recuperate the braking energy under the premise of safety. In pure electric driving mode, the system efficiency is also certain due to the ultimate electric source, i.e., the battery and MG2. Therefore, this paper focuses on the system transmission efficiency for the operation modes that the engine participates in the driving.

The engine operation efficiency η_E reflects the energy conversion efficiency between chemical energy P_{che} and mechanical energy P_E. The conversion efficiency is

$$\begin{cases} P_{che} = \dot{m}_f(\omega_E, T_E) H_{lhv}, \\ P_E = T_E \omega_E, \\ \eta_E = \dfrac{P_{che}}{P_E}, \end{cases} \tag{4}$$

where H_{lhv} is the fuel lower heating value and the engine fuel flow rate $\dot{m}_f$ relates to the engine speed and torque. The efficiencies of MG1 and MG2 denote the conversion between electrical energy and mechanical energy and relate to their torques and speeds.

$$\begin{cases} \eta_G = \varphi_G(\omega_G, T_G), \\ \eta_M = \varphi_M(\omega_M, T_M), \end{cases} \tag{5}$$

where η_G and η_M denote efficiencies of MG1 and MG2, respectively, and φ_G and φ_M are experimental efficiency maps of MG1 and MG2. Both the engine fuel flow rate and efficiencies of the electric machines are described as static look-up tables.

Due to the internal resistance, there are energy losses of the battery during the conversion between chemical energy and electrical energy. The internal resistance R_{int} is determined by the battery state of charge (SOC), temperature t_b, and the battery operation states, which is defined as λ. $\lambda = 1$ and $\lambda = -1$ represent that the battery operates in discharging

and charging state, respectively. The battery resistance is described as

$$R_{\text{int}} = \begin{cases} R_{\text{dis}}(t_{\text{b}}, \text{soc}), & \lambda = 1, \\ R_{\text{chg}}(t_{\text{b}}, \text{soc}), & \lambda = -1. \end{cases} \tag{6}$$

Various modeling methods have been proposed to model the battery SOC [26]. The Rint model of the battery is applied in the paper, i.e.,

$$\dot{\text{soc}} = -\frac{U_{\text{oc}}(t_{\text{b}}, \text{soc}) - \sqrt{U_{\text{oc}}^2(t_{\text{b}}, \text{soc}) - 4P_{\text{bat}}R_{\text{int}}(t_E, \text{soc}, \lambda)}}{2Q_{\text{bat}}(t_{\text{b}})R_{\text{int}}(t_{\text{b}}, \text{soc}, \lambda)}, \tag{7}$$

where P_{bat} is the battery power; U_{oc} denotes the open-circuit voltage, which is influenced by the battery temperature and SOC; and Q_{bat} is the battery capacity.

The battery efficiency η_{bat} is defined as

$$\eta_{\text{bat}} = \begin{cases} \eta_{\text{chg}}, & P_{\text{dc}} > 0, \\ \eta_{\text{dis}}, & P_{\text{dc}} < 0, \end{cases} \tag{8}$$
$$P_{\text{dc}} = P_{G\text{dc}} + P_{\text{Mdc}},$$

where η_{chg} and η_{dis} are the battery efficiencies during charging and discharging process, respectively; P_{dc} is the DC-link power which is affected by the power of MG1 and MG2; and P_{Gdc} is the power transmitted to or from the DC-link related to the mechanical power P_{G} of MG1. When MG1 acts as a generator to generate electricity ($\gamma = 1$, γ denotes the state of the electric machine), the power is transmitted from MG1 to DC-link. When MG1 acts as a motor and consumes electrical energy ($\gamma = -1$), the power flows from the DC-link to MG1. Therefore, we have

$$P_{G\text{dc}} = P_G \eta_G^{\gamma} = T_G \omega_G \eta_G^{\gamma}. \tag{9}$$

Similar definitions are applied to MG2. P_{Mdc} is calculated by

$$P_{\text{Mdc}} = P_{\text{M}} \eta_{\text{M}}^{\gamma} = T_{\text{M}} \omega_{\text{M}} \eta_{\text{M}}^{\gamma}. \tag{10}$$

Consequently, the battery charging and discharging efficiencies are given by

$$\eta_{\text{bat}} = \begin{cases} \eta_{\text{chg}} = \dfrac{P_{\text{bat}}}{P_{\text{dc}}} = \dfrac{U_{\text{oc}} I_{\text{bat}}}{U_{\text{out}} I_{\text{bat}}}, & P_{\text{dc}} < 0, \\ \eta_{\text{dis}} = \dfrac{P_{\text{dc}}}{P_{\text{bat}}} = \dfrac{U_{\text{out}} I_{\text{bat}}}{U_{\text{oc}} I_{\text{bat}}}, & P_{\text{dc}} > 0, \end{cases} \tag{11}$$

where U_{out} is the battery output voltage and I_{bat} is the current of DC-link. According to the battery model, U_{out} is calculated by

$$U_{\text{out}} = \begin{cases} \dfrac{2P_{\text{dc}}R_{\text{dis}}}{U_{\text{oc}} - \sqrt{U_{\text{oc}}^2 - 4P_{\text{dc}}R_{\text{dis}}}}, & P_{\text{dc}} > 0, \\ \dfrac{2P_{\text{dc}}R_{\text{chg}}}{U_{\text{oc}} - \sqrt{U_{\text{oc}}^2 - 4P_{\text{dc}}R_{\text{chg}}}}, & P_{\text{dc}} < 0. \end{cases} \tag{12}$$

Then, the battery charging and discharging efficiencies are

$$\eta_{\text{bat}} = \begin{cases} \eta_{\text{chg}} = \dfrac{U_{\text{oc}}\left(U_{\text{oc}} - \sqrt{U_{\text{oc}}^2 - 4P_{\text{dc}}R_{\text{chg}}}\right)}{2P_{\text{dc}}R_{\text{chg}}}, & P_{\text{dc}} < 0, \\ \eta_{\text{dis}} = \dfrac{2P_{\text{dc}}R_{\text{dis}}}{U_{\text{oc}}\left(U_{\text{oc}} - \sqrt{U_{\text{oc}}^2 - 4P_{\text{dc}}R_{\text{dis}}}\right)}, & P_{\text{dc}} > 0. \end{cases} \tag{13}$$

For any given power of the DC-link, the battery SOC, and temperature, the battery efficiency can be derived. The battery efficiency for different SOC from 0.2 to 0.8 and DC-link power from −80 kW to 80 kW when the battery temperature is 25°C is derived and is shown in Figure 2. It is obvious that the battery efficiency is lower at high power levels. With the increase of DC-link power, the battery SOC shows more obvious influence on the efficiency.

3.2. Powertrain Transmission Efficiency. Based on the aforementioned component efficiencies, the powertrain transmission efficiency which is mainly discussed among the operation modes that the engine is start up is further derived.

For the charging while standstill mode, the fuel is the original source and the battery is the terminal of the energy flow. The powertrain transmission efficiency is written as

$$\eta_{\text{pow}} = \frac{P_{\text{bat}}}{P_{\text{che}}} = \eta_{\text{E}} \eta_{\text{G}} \eta_{\text{bat}}. \tag{14}$$

The engine and MG1 are viewed as engine-generator set. The power of MG2 is zero. Figure 3 describes the powertrain efficiency for the charging while standstill mode when the battery SOC is 0.55 and the temperature is 25°C. It can be seen that the maximal powertrain efficiency is about 0.34, where the operation efficiencies of the engine, MG1, and battery during charging process are counted. Due to the physical limitations of MG1 and engine, some engine operation regions cannot be achieved, as shown by the blank space in Figure 3. By comparing Figures 3 and 4, it is shown that the highest transmission efficiency region corresponds to the region of the engine map with low fuel consumption rate. However, this region also results in large battery charging power, which contributes to the rapid rise of battery SOC. Consequently, the charging while standstill mode is recommended to be activated when the SOC is at a relative low level, for example, below 0.4.

As for hybrid driving mode, the origin and terminal of the energy flow vary with the battery states. When the battery assists the engine to drive the vehicle ($P_{\text{bat}} > 0$), it acts as a power source. All the energy that originates from the engine fuel and battery flows to the vehicle output shaft. However, when the battery is charged, the energy that originates from the engine fuel flows to the battery and the vehicle output shaft. Depending on the battery state in hybrid driving mode, the powertrain transmission efficiency is

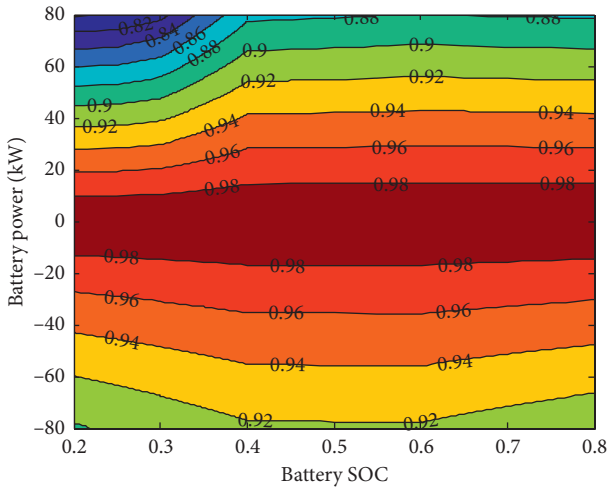

Figure 2: The battery efficiency at the temperature of 25°C.

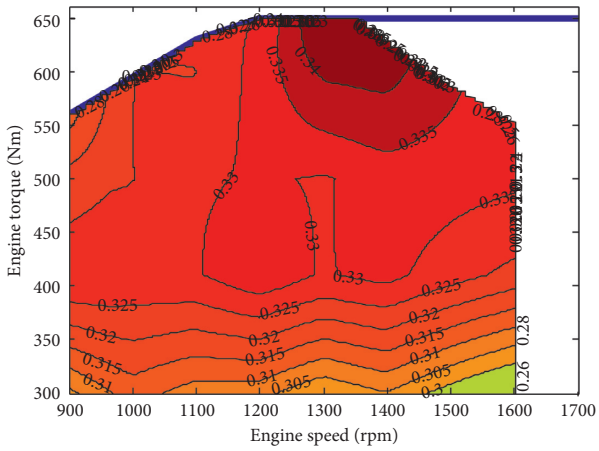

Figure 3: The powertrain efficiency for charging while standstill mode.

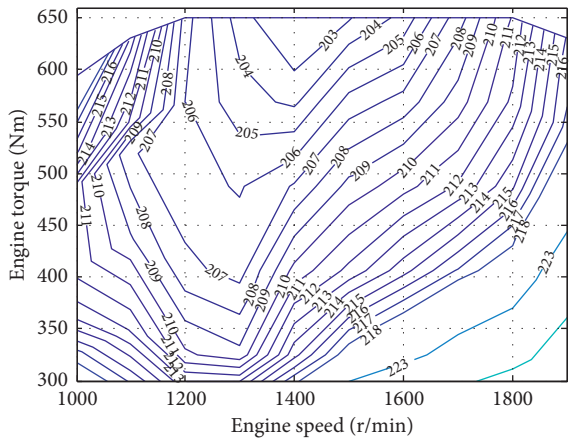

Figure 4: Engine map.

$$\eta_{pow} = \begin{cases} \dfrac{P_{out}}{P_{che} + P_{bat}}, & P_{dc} > 0, \\ \dfrac{P_{out} - P_{bat}}{P_{che}}, & P_{dc} < 0. \end{cases} \tag{15}$$

The mechanical output power at the shaft is

$$P_{out} = T_{out}\omega_{out}. \tag{16}$$

When the battery assists in driving the vehicle, it is obvious that the more assistance power the battery provides, the higher the powertrain transmission efficiency is because the battery and motor efficiencies are much higher than the engine. However, it ignores the fact that the consumed electrical energy must be replenished by the engine power in the future. The energy loss will occur in the engine, MG1, and battery during the future charging process. Meanwhile, the power charged in the battery should also discharge in the future to maintain the battery charging sustainability [27]. Consequently, in order to account for the battery charging and discharging in the future, the battery power is corrected and calculated by

$$P_{bat} = \begin{cases} P_{dc}\left(\eta_{bat}\eta_{av\_chgp}\right)^{-1}, & P_{dc} > 0, \\ P_{dc}\eta_{bat}\eta_{av\_disp}, & P_{dc} < 0, \end{cases} \tag{17}$$

where η_{av_disp} and η_{av_chgp} denote the estimated average efficiencies for the future discharging and charging process. They are defined as

$$\begin{cases} \eta_{av\_chgp} = \overline{\eta}_{E}\overline{\eta}_{elechg}\overline{\eta}_{bchg}, \\ \eta_{av\_disp} = \overline{\eta}_{eledis}\overline{\eta}_{bdis}, \end{cases} \tag{18}$$

where $\overline{\eta}_{E}$, $\overline{\eta}_{elechg}$, and $\overline{\eta}_{bchg}$ represent the average efficiencies of the engine, electric machine, and the battery when the battery is charged by part of the engine energy, while $\overline{\eta}_{eledis}$ and $\overline{\eta}_{bdis}$ represent the average efficiencies of the electric machine and the battery when the battery discharges in the future. Although the efficiencies of different components are time varying, they are difficult to be estimated in real time and constant average values can be adopted for simplification [13]. In combination of Figures 2 and 3, the average charging efficiency η_{av_chgp} and discharging efficiency η_{av_disp} are chosen to be 0.33 and 0.96, respectively.

4. Optimization of Energy Management Strategy

The operation mode of the power split HEV should be decided and the output torque of different power sources is further calculated. The powertrain control scheme is described in Figure 5. The controller calculates the desired engine torque T_E^*, MG1 torque T_G^*, MG2 torque T_M^*, and the braking torque T_{brk}^* according to the required torque T_{req} and velocity v_{req}, as well as the system states, such as the

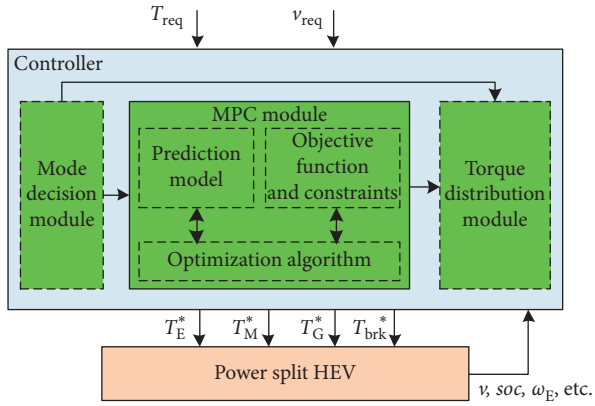

Figure 5: Energy management scheme.

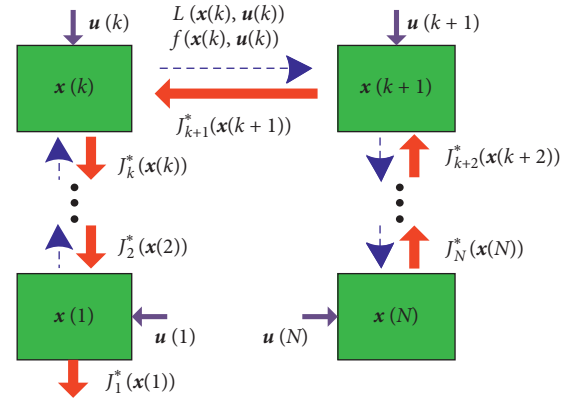

Figure 6: The schematic diagram of DP implementation.

actual velocity v, the battery SOC, and engine speed. The mode decision module is used online to identify the operation mode of the HEV according to some predefined thresholds. Then, model predictive control module designed for the operation mode that the engine is start up is applied online to obtain the engine speed and torque with optimal powertrain transmission efficiency as objective function. The torque distribution module calculates the torque of electric machines and the friction braking. It is worth noting that when the engine is shut down, the torque distribution module directly calculates the torques of MG1, MG2, and/or the friction braking torque without activating the MPC module.

The predefined thresholds in the mode decision module, such as the vehicle speed and acceleration, strongly affect the HEV mode switching. Therefore, the global optimal control sequences under different driving cycles that ensure exact battery charging sustainability are firstly derived offline. Based on the offline optimized results, the thresholds are derived and stored in the mode decision module to guide the online mode switching.

4.1. Mode Decision Module. When the vehicle speed and acceleration are within an appropriate range during driving process, MG2 can provide enough torque and the HEV operates in pure electric driving mode. Therefore, if the battery SOC is higher than a certain value SOC_{lo}, the vehicle is just driven by MG2 and the engine is shut down. Otherwise, the engine engages in the driving. When the vehicle stops, the engine will drive MG1 if the battery SOC is smaller than a certain value SOC_{ch}. During braking, the regenerative braking strategy is also certain for maximal energy regeneration.

DP algorithm, based on the Bellman principle of optimality, is implemented offline to derive the global optimal solutions. The principle of DP algorithm is shown in Figure 6. The time horizon is discretized into N steps and the optimal policy of DP is obtained by solving the multistage decision-making problems of backward optimization from the terminal stage.

For any stage (time step), the state relies on the former state and relevant control variable, that is,

$$\mathbf{x}(k+1) = f(\mathbf{x}(k), \mathbf{u}(k)). \tag{19}$$

In our study, the state variable is the battery SOC, and control variables include the engine torque and speed.

$$\begin{aligned} \mathbf{x} &= [\text{soc}], \\ \mathbf{u} &= [T_E \ \ \omega_E]. \end{aligned} \tag{20}$$

In the backward direction, the cost-to-go function that starts from the N_{th} stage is defined as

$$J_N^*(\mathbf{x}(N)) = 0, \tag{21}$$

$$J_k^*(\mathbf{x}(k)) = \min_{u(k)} \left[L(\mathbf{x}(k), \mathbf{u}(k)) + J_{k+1}^*(\mathbf{x}(k+1)) \right], \tag{22}$$

where $J*k(\mathbf{x}(k))$ is the optimal cost-to-go function from the k_{th} stage to the final stage and $L(\mathbf{x}(k), \mathbf{u}(k))$ is the cost-to-go function from the k_{th} stage to the $(K+1)_{th}$ stage for certain state and control variables. By converting the global optimal problem into a series of staged suboptimal problems, the global optimal solutions Π^* should ensure minimal $J*(\mathbf{x}(1))$, i.e.,

$$\prod^* = \arg\min J_1^*(\mathbf{x}(1)). \tag{23}$$

For a complete cycle, the best operation state is that the initial SOC equals to the final value, which means that exact battery sustainability is maintained. In practical applications, the vehicle future velocities cannot be predicted precisely. Without a priori knowledge of the velocity profile, the exact battery balance condition is difficult to realize. However, for offline applications, the global optimization strategy for certain cycles can be analyzed and applied as benchmarks to evaluate other instantaneous optimal strategies. The exact battery sustainability can also be ensured. Consequently, minimal engine fuel consumption is selected as the objective.

$$L(\mathbf{x}(k), \mathbf{u}(k)) = \dot{m}_f(\mathbf{x}(k), \mathbf{u}(k))\Delta T, \tag{24}$$

where ΔT is the time step.

The exact battery SOC balance is set as constraints. Besides, the physical constraints of the engine and electric machines should also be addressed. The constraints for the global optimization problem is

$$\begin{cases} \mathrm{soc}(0) = \mathrm{soc}(N), \\ \omega^{\mathrm{E}}_{\min} \le \omega_{\mathrm{E}} \le \omega^{\mathrm{E}}_{\max}, \\ T^{\mathrm{E}}_{\min}(k) \le T_{\mathrm{E}} \le T^{\mathrm{E}}_{\max}, \\ \omega^{\mathrm{G}}_{\min} \le \omega_{\mathrm{G}} \le \omega^{\mathrm{G}}_{\max}, \\ T^{\mathrm{G}}_{\min}(k) \le T_{\mathrm{G}} \le T^{\mathrm{G}}_{\max}, \\ \omega^{\mathrm{M}}_{\min} \le \omega_{\mathrm{M}} \le \omega^{\mathrm{M}}_{\max}, \\ T^{\mathrm{M}}_{\min}(k) \le T_{\mathrm{M}} \le T^{\mathrm{M}}_{\max}, \end{cases} \tag{25}$$

where $\omega^{\mathrm{E}}_{\min}$ and $\omega^{\mathrm{E}}_{\max}$ are the minimal and maximal engine speed. Similar definitions are applied to other maximal and minimal torques and speeds.

Some driving cycles that are common for heavy-duty buses, such as the CTBCDC (China Transit Bus City Driving Cycle), the OCC (Orange County Bus Cycle), and the WLTC (Worldwide harmonized Light vehicles Test Cycle) for Class 1 vehicle, are tested with DP to analyze the engine operation. The velocity profiles of different cycles are shown in Figure 7.

The road grade is ignored. The required torque ultimately depends on the vehicle speed and acceleration. Figure 8(a) gives the vehicle operation modes for different velocities and accelerations under the combined cycle of CTBCDC, OOC, and WLTC, where the yellow squares represent the conditions that the engine is start up and the blue squares denote the conditions that the engine is shut down. The probability cloud that the HEV operates in pure electric driving mode during driving process is also introduced and given in Figure 8(b) to better determine the thresholds. In the figure, the color means the probability that the vehicle operates in pure electric driving mode for the whole combined driving cycle, and the value is shown by the color bar in the figure. It can be concluded that the larger the probability is, the vehicle is more likely to operate with the corresponding acceleration and velocity, and the HEV is also more likely to operate in pure electric driving mode. Figure 8(b) reflects the degree of the vehicle operation with certain acceleration and velocity. By combing the two figures, the critical points for the mode switching during driving are obtained. The coordinates of these points are A (0, 1.1), B (12, 1.1), C (12, 0.45), D (24, 0.45), E (24, 0.2), F (44, 0.2), and G (44, 0). It is seen that there are some points beyond the boundary which indicates that the vehicle should have been in pure electric driving mode, as shown in Figure 8(a). However, since the appearance frequency of these points is small, as shown by the corresponding probability in Figure 8(b), these points can be attributes to the region that the engine is started up.

4.2. MPC Module. When the engine is start up, MPC is used to derive the engine torque and speed. The required vehicle torque and velocity in the prediction horizon are necessary to be predicted. Different kinds of prediction methods, such as neural network and exponential prediction rules, have been used to predict the torque and/or velocity. One-step Markov is applied to predict the required torque. Then, the vehicle velocity sequence is obtained. The solving method presented in ADVISOR is adopted to calculate the prediction velocity:

$$\begin{cases} av = 0.5\rho_{air} C_d A_f, \\ bv = \dfrac{2m}{\Delta T}, \\ cv = mg(f\cos\theta + \sin\theta) - \dfrac{2mv_{cur}}{\Delta T} - \dfrac{T_{\mathrm{req}}}{R_w}, \\ v_{avg} = \dfrac{\left(-bv + \sqrt{bv^2 - 4av \cdot cv}\right)}{2av}, \\ v_{next} = 2v_{avg} - v_{cur}, \end{cases} \tag{26}$$

where v_{cur} and v_{next} are the vehicle velocities for the current and next moment, respectively, and v_{avg} denotes the average speed for the current step.

The torque is predicted according to the current torque and the one-step Markov matrix which describe the transition probability from the torque state $T_{\mathrm{req}i}$ to the other one $T_{\mathrm{req}j}$. The one-step Markov matrix is constructed using optimal nearest neighbor and maximum likelihood method after the continuous required torque for certain driving cycles is discretized into finite elements [28].

$$\begin{aligned} m_i &= \sum_{j=1}^{N} m_{ij}, \\ P_{ij}(1) &= \frac{m_{ij}}{m_i}, \end{aligned} \tag{27}$$

where m_i is the total transition numbers start from the torque state $T_{\mathrm{req}i}$; m_{ij} represents the transition frequency from $T_{\mathrm{req}i}$ to $T_{\mathrm{req}j}$; and $P_{ij}(1)$ is the one-step torque transition probability.

The objective of the MPC is to maximize the powertrain transmission efficiency. The actual battery SOC should also be controlled within an acceptable range to maintain the battery charging sustainment. Therefore, the maximization of the powertrain transmission efficiency and the minimization of the deviation between the actual and reference battery SOC are chosen as the control targets. The optimal problem is described as

$$\begin{aligned} J = \min \sum_{k=0}^{Nt-1} & \begin{bmatrix} r_{ref}\left(\eta_{pow}(k) - \eta_{ref}\right)^2 \\ + r_{soc}\left(\mathrm{soc}(k) - \mathrm{soc}_{ref}\right)^2 \end{bmatrix}, \\ \text{s.t.} & \begin{cases} \omega^{\mathrm{E}}_{\min} \le \omega_{\mathrm{E}} \le \omega^{\mathrm{E}}_{\max}, \\ T^{\mathrm{E}}_{\min}(k) \le T_{\mathrm{E}} \le T^{\mathrm{E}}_{\max}, \\ \omega^{\mathrm{G}}_{\min} \le \omega_{\mathrm{G}} \le \omega^{\mathrm{G}}_{\max}, \\ T^{\mathrm{G}}_{\min}(k) \le T_{\mathrm{G}} \le T^{\mathrm{G}}_{\max}, \\ \omega^{\mathrm{M}}_{\min} \le \omega_{\mathrm{M}} \le \omega^{\mathrm{M}}_{\max}, \\ T^{\mathrm{M}}_{\min}(k) \le T_{\mathrm{M}} \le T^{\mathrm{M}}_{\max}, \end{cases} \end{aligned} \tag{28}$$

where N_t is the prediction horizon; η_{ref} is defined as the reference efficiency and is set to be 0.4 which is larger than the maximal powertrain transmission efficiency η_{ref} because

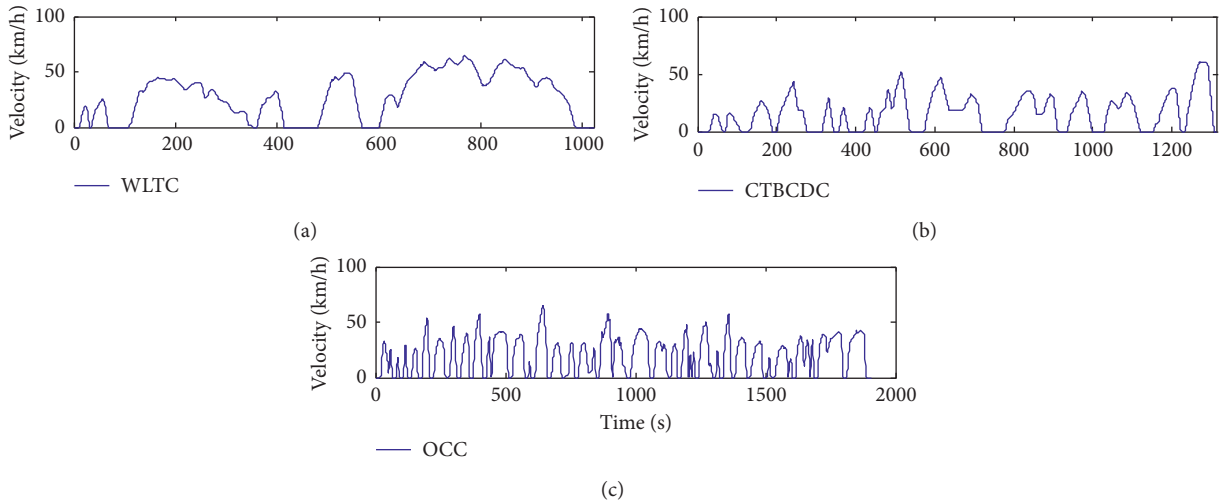

Figure 7: Velocity profiles of different cycles.

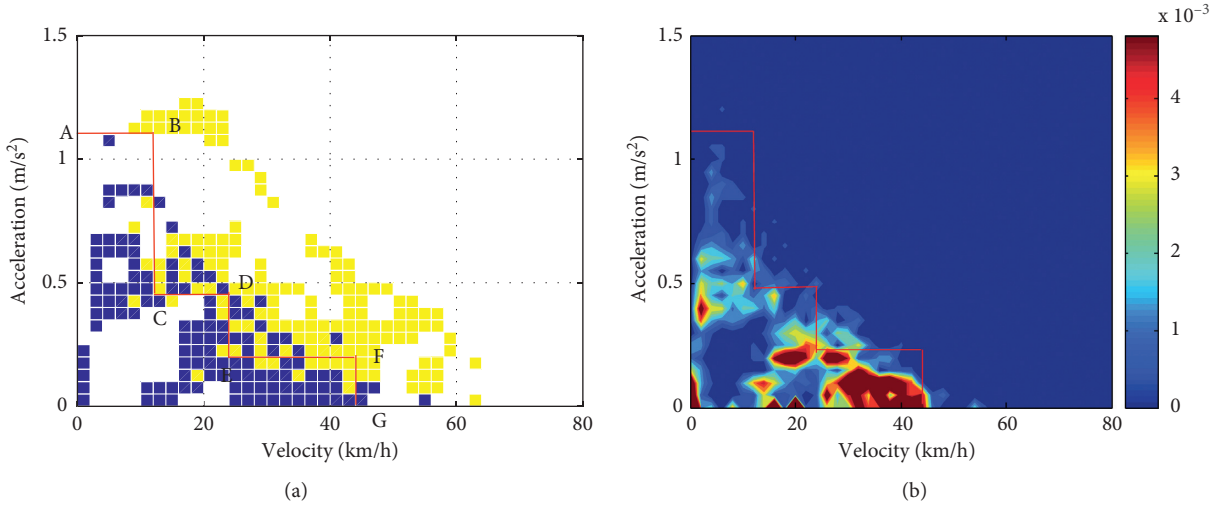

Figure 8: Operation modes of the HEV for different velocities and accelerations. (a) Operation modes during driving. (b) The probability cloud that the HEV operates in pure electric driving.

η_{pow} needs to be maximized; and r_{eff} and r_{soc} are weighting factors of the transmission efficiency and the battery SOC, respectively.

Then, the optimal control sequence in the prediction horizon is derived according to equations (19)~(28). Only the first engine torque and speed are implemented into the plant. For the next receding horizon, the calculation of the optimal results is repeated. The solving process of MPC controller using DP algorithm is shown in Figure 9.

4.3. Torque Distribution Module. When MG2 is the only power source of the vehicle, the torque of MG2 is

$$T_M = \frac{T_{out}}{1 + K_2}. \tag{29}$$

When the engine is start up, the torques of two electric machines are calculated by

$$\begin{cases} T_G = -\dfrac{1}{1 + K_1} T_E, \\ T_M = \dfrac{T_{out}}{1 + K_2} - \dfrac{K_1 T_E}{(1 + K_1)(1 + K_2)}. \end{cases} \tag{30}$$

During braking, for simplification, the mechanical braking mode is incorporated in the regenerative braking mode. The friction braking torque is

$$T_{brk} = T_{out} - (1 + K_2) T_M. \tag{31}$$

5. Simulation Analysis

The weighting factors of the powertrain efficiency and the battery SOC are set to be 1 and 1500, respectively. The prediction horizon is set to be 6 s. The step size of the

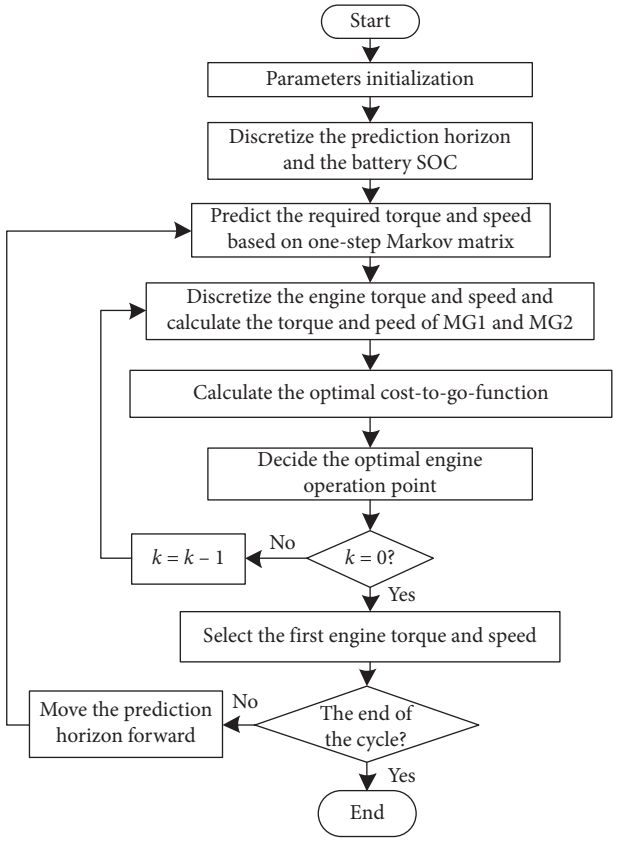

Figure 9: The solving process of MPC controller using DP algorithm.

simulation model is 0.1 s, which is enough to evaluate the vehicle fuel economy, while the step size of the MPC controller is 1 s. The thresholds that determine the HEV operations modes are illustrated in Section 4.1.

Simulations under the CTBCDC, WLTC, and OOC driving cycles are performed to evaluate the effectiveness of the proposed transmission efficiency oriented predictive strategy (TEOPS). The proposed strategy is compared with a kind of rule-based strategy inspired by the Toyota Prius control strategy [29, 30]. In the rule-based controller, the battery charging sustainability is maintained by introducing the battery balancing power which is obtained by a PI controller. The inputs of the PI controller are the actual and reference SOC values. The proportional and integral coefficients are 4×10^6 and 2×10^3, while the reference SOC is 0.55. For brevity, only the time responses under CTBCDC and OOC scenarios are presented.

Figure 10 presents the battery trajectories under CTBCDC and OOC. Since the battery SOC is constrained by the objective function in TEOPS and the PI controller in the rule-based strategy, the battery SOC fluctuates along the reference value for both driving cycles. Good battery charging sustainability is maintained. Consequently, the battery operates in high efficiency regions. Since the rule-based strategy applies hard SOC constraints with the PI controller for the whole time history, while the proposed TEOPS only constrains the SOC for the operation modes that the engine is start up (the battery SOC in TEOPS is strongly affected by the operations modes for the whole time history), the change of the battery SOC with TEOPS is larger than the SOC change with the rule-based strategy.

Figures 11 and 12 give the time responses of different powertrain components. The ring gear of PG2 is fixed. As a result, the rotational speed of MG2 is proportional to the vehicle speed shown in Figure 7 and is not presented in this section. From the figures, it can be seen that all components are controlled to be within their physical limitations. Compared with rule-based strategy, the proposed strategy leads to larger torque and speed of the engine for CTBCDC. Based on the thresholds derived through global optimization, there is more rest time of the engine with TEOPS. However, since the OOC consists of frequent acceleration and deceleration, while CTBCDC is modal type cycle which is determined through statistical analysis of numerous static data, there are more frequent engine starts and stops under OOC. When the engine is shut down, the rotational direction of MG1 is contrary to the wheel rotation direction due to the mechanical connection between MG1 and the vehicle output shaft, as shown in Figures11(b) and 11(d), 12(b) and 12(d). More specifically, it can be concluded by the static torque and speed relations within the power coupling device, as described in equations (30) and (32). When the engine is start up and the vehicle speed is not high, the rotational directions of the engine and MG1 will be the same, as described by equation (32). Therefore, the power of MG1 is negative and MG1 mainly converts part of the engine output energy into electric energy. The torque of MG2 is either positive or negative, while the rotational direction of MG2 is always the same as that of the output shaft. During braking, MG2 acts as a generator to recycle the braking energy. In the driving process, when the engine torque is large enough and the required driving torque at the output shaft is small, the torque of MG2 will be negative. Since the rotational speed of MG2 is always positive (without considering the reverse scenario), the power of MG2 is negative and MG2 works as a generator. Otherwise, MG2 consumes electrical energy to drive the vehicle as the assisted power source of the engine.

$$\begin{cases} (1+K_1)\omega_{\mathrm{E}} = \omega_{\mathrm{G}} + K_1\omega_{\mathrm{out}}, \\ (1+K_2)\omega_{\mathrm{out}} = \omega_M. \end{cases} \tag{32}$$

The powertrain transmission efficiencies for CTBCDC and OOC are shown in Figure 13. It is obvious that the proposed TEOPS ensures larger powertrain transmission efficiency for most time regions. However, there are still some time regions that higher transmission efficiency is achieved by the rule-based strategy. It is because that the first control variable derived by MPC is used to maintain the optimal transmission efficiency for the prediction horizon, but the transmission efficiency for the current moment may not be optimal. Besides, the results are also influenced by the discrete grids of state and control variables in the DP optimization. In order to ensure good real-time capability, the number of discrete grids is not large and thus affects the accuracy of the optimal solutions.

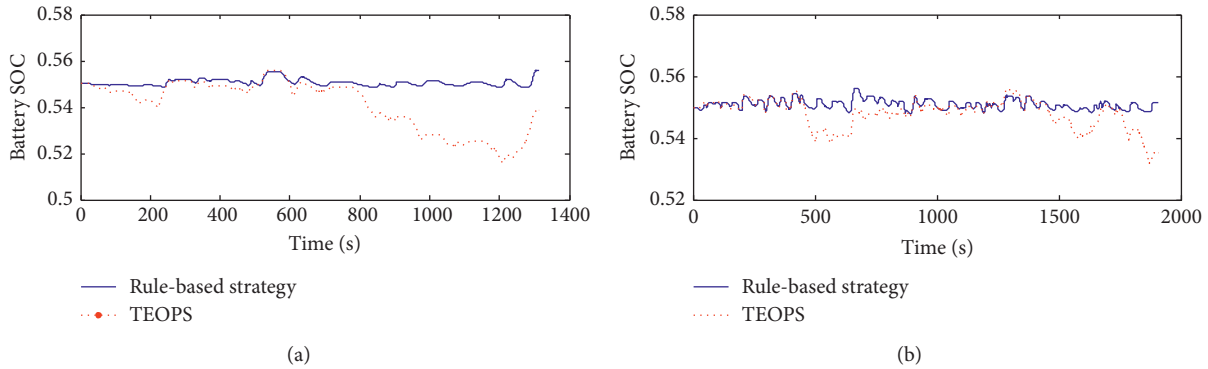

Figure 10: Battery SOC under different cycles. (a) CTBCDC. (b) OCC.

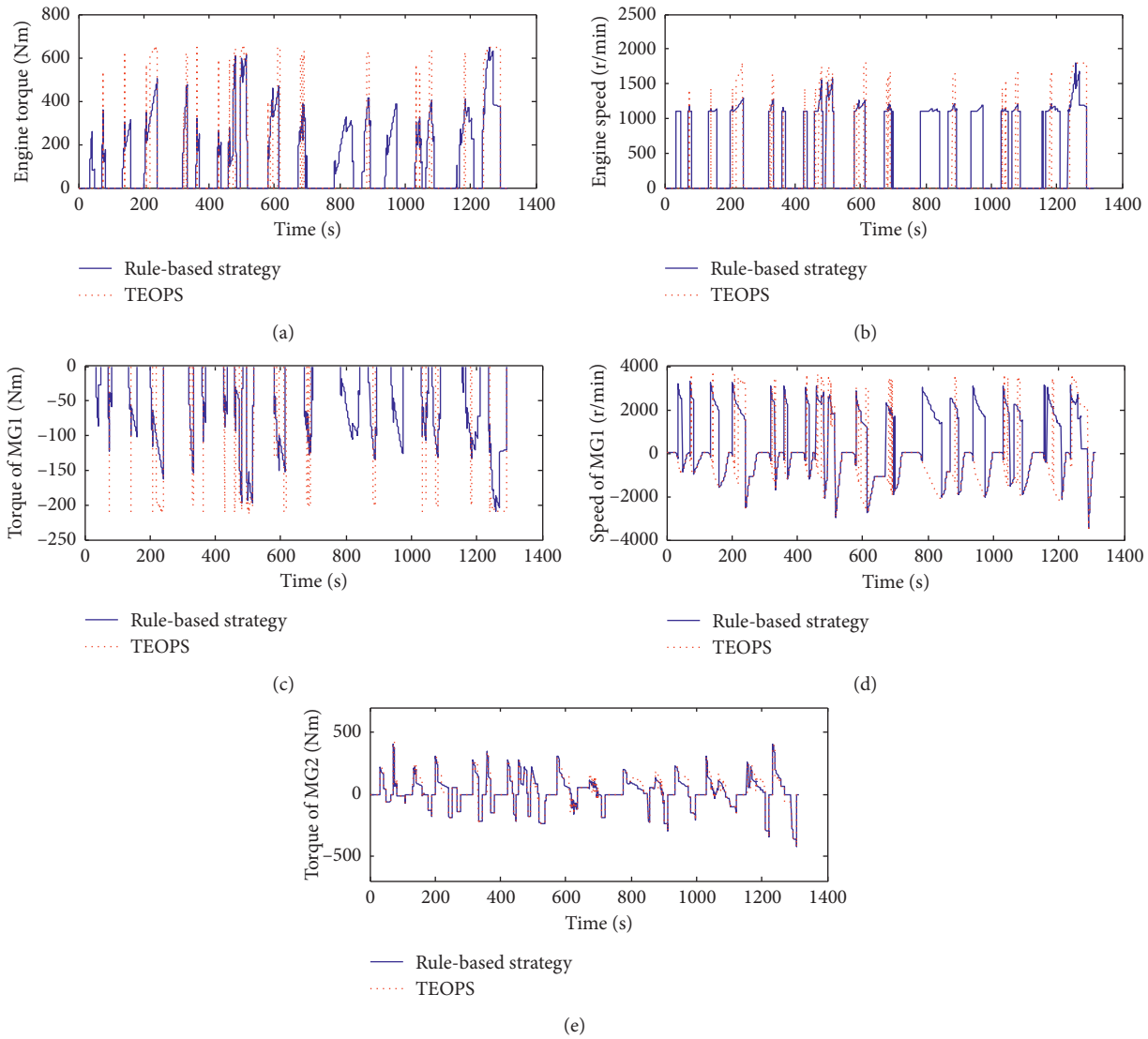

Figure 11: Time responses under CTBCDC. (a) Engine torque. (b) Engine speed. (c) Torque of MG1. (d) Speed of MG1. (e) Torque of MG2.

The proposed TEOPS is also compared with the equivalent consumption minimization strategy (ECMS) which is capable of realizing instantaneous optimization. In the ECMS, the minimization of the engine fuel consumption is substituted with the instantaneous minimization of the cost as shown in the following equation:

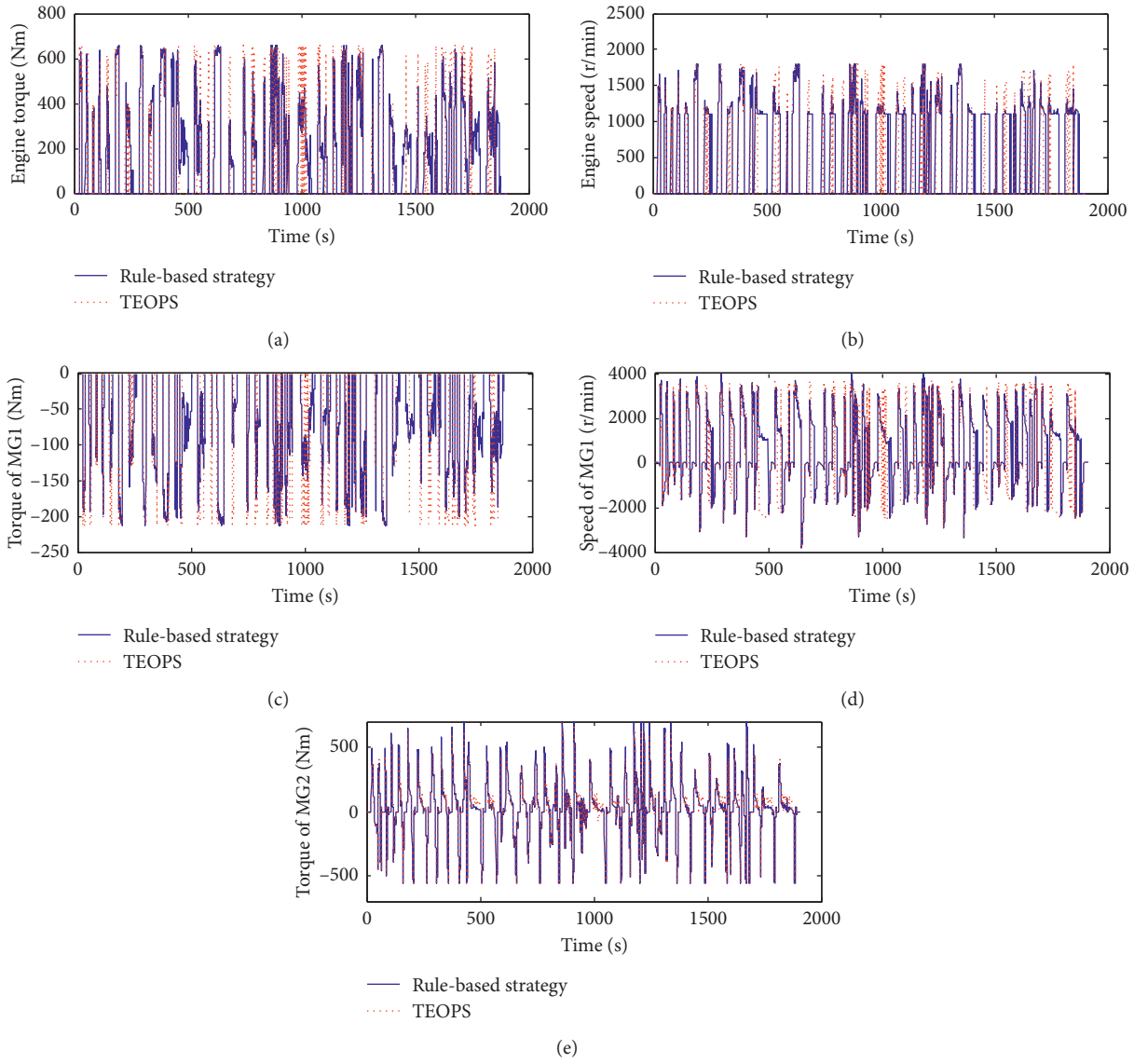

Figure 12: Time responses under OOC. (a) Engine torque. (b) Engine speed. (c) Torque of MG1. (d) Speed of MG1. (e) Torque of MG2.

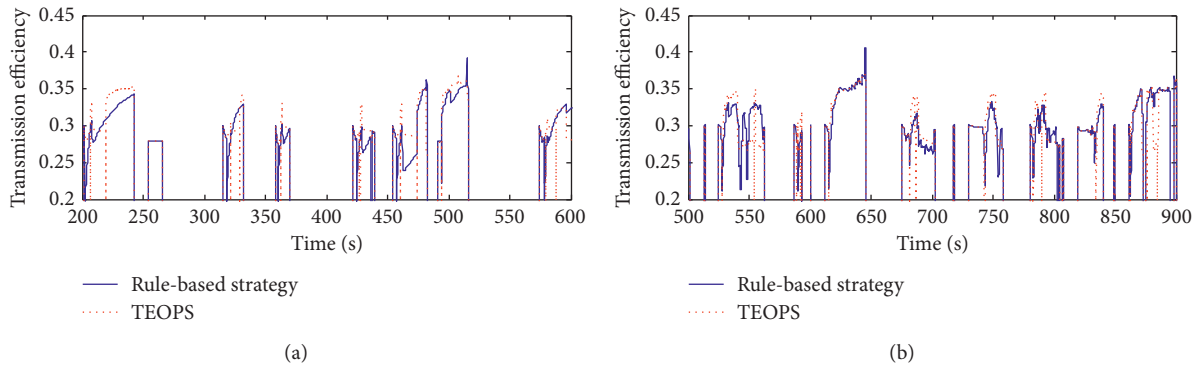

Figure 13: Powertrain transmission efficiency under different cycles. (a) CTBCDC. (b) OOC.

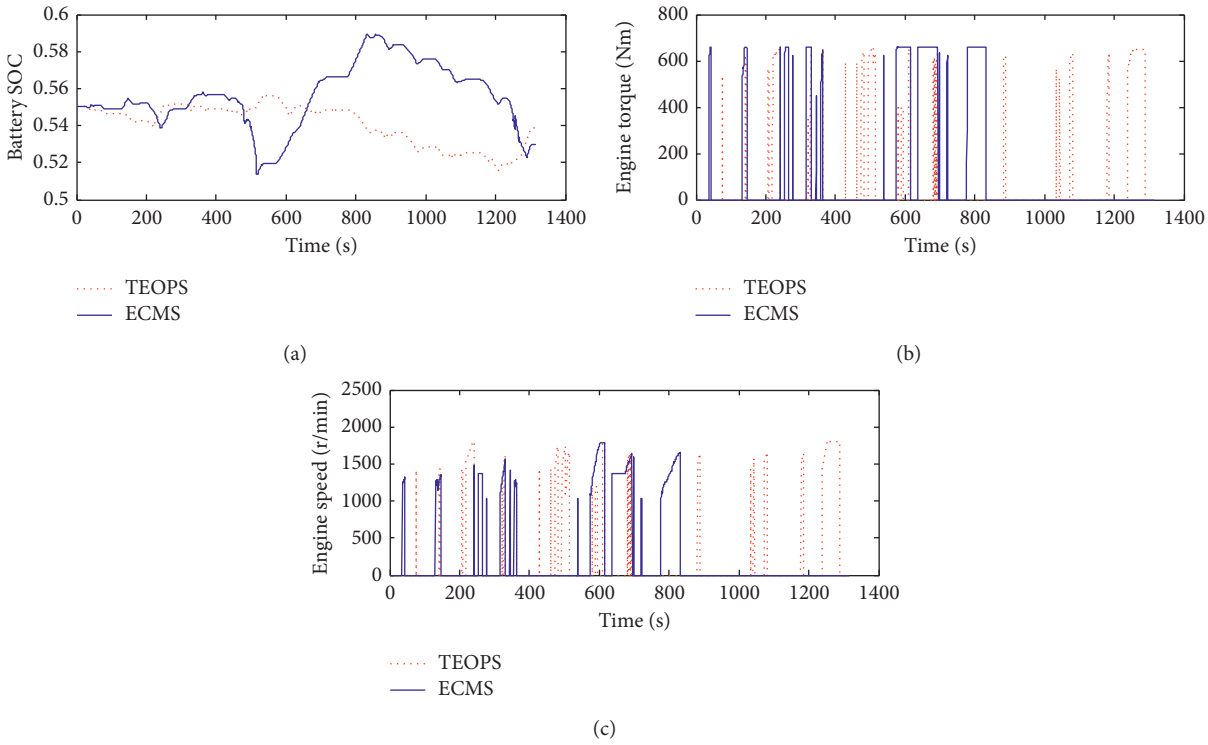

Figure 14: Time responses under CTBCDC with ECMS and TEOPS. (a) Battery SOC. (b) Engine torque. (c) Engine speed.

$$\dot{m}_{f\_\text{total}} = \dot{m}_f + f_{\text{pen}}\dot{m}_{\text{batt}}, \tag{33}$$

$$f_{\text{pen}} = \left(1 - x_{\text{SOC}}^3\right) + \gamma_{\text{SOC}}\left(-\int_0^{t_f} x_{\text{SOC}}\,\mathrm{d}t\right), \tag{34}$$

$$x_{\text{SOC}} = \frac{0.5\text{soc} - \left(\text{SOC}_{\max} + \text{SOC}_{\min}\right)}{\left(\text{SOC}_{\max} - \text{SOC}_{\min}\right)}, \tag{35}$$

where $\dot{m}_{f\_\text{total}}$ is the cost; f_{pen} is the penalty related to the battery equivalent fuel consumption rate $\dot{m}_{\text{batt}}$; $\text{SOC}_{\max}$ and $\text{SOC}_{\min}$ are the upper and lower SOC limits; and γ_{SOC} is the coefficient. The derivation of the battery equivalent fuel consumption rate is detailed in Ref. [9].

Time responses of the battery and the engine under CTBCDC with ECMS and TEOPS are given in Figure 14. It can be seen that the ECMS can also maintain the battery charging sustainability well because the actual battery SOC is introduced into the penalty f_{pen} to penalize the electrical energy consumption, as shown in equations (34) and (35). However, since it is the upper and lower SOC limits instead of the deviation between the actual and reference SOC that are used to constrain the battery variation, the change degree of the SOC with ECMS is larger than the value with TEOPS. It is observed that ECMS also ensures the engine to operate within the physical limitations. Compared with TEOPS, there are less starts and stops of the engine when ECMS is applied. Especially after 800 s, the vehicle is solely driven by MG2. In such a manner, the final battery SOC is controlled to be within a certain range.

The powertrain transmission efficiency is shown in Figure 15. It is observed that the engine output torque is large with ECMS and the powertrain transmission efficiency

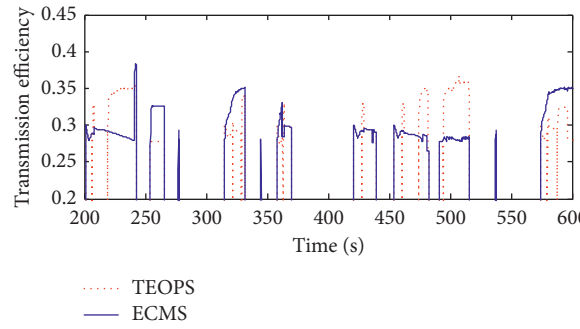

Figure 15: Powertrain transmission efficiency under CTBCDC with ECMS and TEOPS.

for these time regions is also high because the engine with larger torque demonstrates higher operation efficiency. The powertrain transmission efficiency with TEOPS is lower than the value with ECMS in some time regions. This is because the first control variable derived by the MPC-based TEOPS only maintains the optimal efficiency for the prediction horizon instead of the current moment. Meanwhile, the larger average output torque of the engine with ECMS ensures high efficiency. However, larger average output torque when the engine is engaged in the driving also results in longer operation of pure electric driving because of the requirements for battery charging sustainability. It can be seen from Figures 14(b) and 15 that when the engine torque is zero during driving process (pure electric driving), the powertrain transmission efficiency is in a low level due to the consideration of future charging efficiency. Therefore, although the instantaneous powertrain transmission efficiency

Table 2: Fuel economy of the vehicle for different initial SOC values.

Driving cycle	Initial SOC	Rule-based strategy			ECMS			TEOPS		
		SOC_{fin}	m_f/L	m_{equ}/L	SOC_{fin}	m_f/L	m_{equ}/L	SOC_{fin}	m_f/L	m_{equ}/L
CTBCDC	0.60	0.550	14.45	24.30	0.565	17.08	23.94	0.557	13.57	22.04
	0.55	0.556	22.08	20.90	0.530	18.35	22.29	0.541	17.82	19.59
WLTC-Class 1	0.60	0.548	13.53	20.98	0.569	15.06	19.50	0.554	13.20	19.79
	0.55	0.551	19.24	19.10	0.535	17.22	19.37	0.554	18.04	17.47
OOC	0.60	0.545	21.28	27.34	0.557	23.23	27.97	0.535	21.26	28.32
	0.55	0.552	27.68	27.46	0.525	24.11	26.86	0.535	24.24	25.89

with ECMS is higher than the efficiency with TEOPS in some time regions, in terms of the whole time history, the TEOPS shows better performance in improving the system transmission efficiency.

Table 2 compares the vehicle fuel economy with different strategies, where SOC_{fin} is the SOC at the end of the driving cycle. m_f and m_{equ} represent the engine fuel consumption and the equivalent fuel consumption for 100 kilometers. The equivalent fuel consumption treats the electric energy consumption of the battery as equivalent engine fuel. As illustrated by Table 2, the engine shows less fuel consumption with higher initial SOC values. Because the reference SOC is set to 0.55, when the initial SOC value is larger, for example, 0.6, there is larger discharging energy of the battery, which leads to less consumption of the engine fuel. It can also be inferred that, compared with the discharging scenario, there will be more engine fuel consumption when the battery is charged. When the battery initial SOC value is 0.6, although the engine fuel consumption with TEOPS is slightly reduced, the equivalent fuel consumption is increased due to more battery energy consumption (the finial battery SOC with TEOPS is 0.535 while that with rule-based strategy and ECMS is 0.545 and 0.557, respectively). The engine fuel consumption alone is not adequate to reflect the actual vehicle fuel economy. Therefore, the equivalent fuel consumption which accounts for the battery discharging and charging is also compared in the paper. As shown in Table 2, compared with the rule-based strategy, both the engine fuel consumption and the equivalent fuel consumption are reduced to different degrees for most simulation scenarios with the proposed TEOPS, except for when the battery initial SOC is 0.6 under OOC. The rule-based strategy in our study imposes the battery SOC correction and the engine start/stop logic and can realize good fuel economy with well-tuned parameters [29, 30]. By comparing the rule-based strategy and the ECMS, it can be observed that ECMS does not demonstrate obvious benefits in reducing engine fuel consumption and improving the equivalent fuel economy than the well-tuned rule-based strategy. In general, the proposed TEOPS strategy demonstrates favourable control effects by comparing the simulation results of the three different strategies.

6. Conclusions

The operation efficiency of the engine, electric machines, and the battery for a power split HEV with planetary gear sets are analyzed. On this basis, the powertrain transmission efficiency considering future battery charging and discharging when the engine is start up is derived. The controller that yields better mode decision and powertrain transmission efficiency is designed and investigated. In the controller, the mode decision thresholds are optimized offline based on global optimization results derived by DP algorithm. Model predictive control, which also applies DP algorithm in the finite prediction horizon, is used online to calculate the optimal solutions which can maximize the powertrain transmission efficiency for the operation modes that the engine is start up.

The rule-based strategy which is inspired by the Toyota Prius control principle and the ECMS which can realize instantaneous optimization is adopted as comparisons to highlight the advantages of the proposed strategy. Simulation studies under different driving cycles are conducted which validate the superiorities of proposed TEOPS. Compared with rule-based strategy and the ECMS, the proposed strategy ensures high powertrain transmission efficiency. As a result, the equivalent fuel economy of the power split HEV with the proposed strategy can be effectively improved. Commendable benefits of the transmission efficiency oriented predictive energy management strategy are highlighted.

Data Availability

The data used to support the findings of this study are available from the corresponding author upon request.

Conflicts of Interest

The authors declare that they have no conflicts of interest.

Acknowledgments

This project was funded by the National Natural Science Foundation of China (grant nos. 51575238 and U1764257), the Postdoctoral Science Foundation of China (grant no. 2019M661752), the Natural Science Foundation of Jiangsu Province (grant nos. BK20190844 and BK20180100), the Natural Science Research Project of Jiangsu Higher Education Institutions (grant nos. 19KJB580001 and 18KJB580001), and the Six Talent Peaks Project of Jiangsu Province (2018-TD-GDZB-022).

References

[1] J. Hu, B. Mei, H. Peng, and X. Jiang, "Optimization design and analysis for a single motor hybrid powertrain configuration with dual planetary gears," *Applied Sciences*, vol. 9, no. 4, p. 707, 2019.

[2] D. Shi, P. Pisu, L. Chen, S. Wang, and R. Wang, "Control design and fuel economy investigation of power split HEV with energy regeneration of suspension," *Applied Energy*, vol. 182, pp. 576–589, 2016.

[3] K. Ç Bayindir, M. A. Gözüküçük, and A. Teke, "A comprehensive overview of hybrid electric vehicle: powertrain configurations, powertrain control techniques and electronic control units," *Energy Conversion and Management*, vol. 52, no. 2, pp. 1305–1313, 2011.

[4] F. Wang, J. Zhang, X. Xu, Y. Cai, Z. Zhou, and X. Sun, "New method for power allocation of multi-power sources considering speed-up transient vibration of planetary power-split HEVs driveline system," *Mechanical Systems and Signal Processing*, vol. 128, pp. 1–18, 2019.

[5] J. M. Miller, "Hybrid electric vehicle propulsion system architectures of the e-CVT type," *IEEE Transactions on Power Electronics*, vol. 21, no. 3, pp. 756–767, 2006.

[6] Z. Chen, R. Xiong, and J. Cao, "Particle swarm optimization-based optimal power management of plug-in hybrid electric vehicles considering uncertain driving conditions," *Energy*, vol. 96, pp. 197–208, 2016.

[7] F. Wang, J. Zhang, X. Xu, Y. Cai, Z. Zhou, and X. Sun, "A comprehensive dynamic efficiency-enhanced energy management strategy for plug-in hybrid electric vehicles," *Applied Energy*, vol. 247, pp. 657–669, 2019.

[8] S. H. Wang, S. Zhang, D. H. Shi et al., "Research on instantaneous optimal control of the hybrid electric vehicle with planetary gear sets," *Journal of the Brazilian Society of Mechanical Sciences and Engineering*, vol. 41, no. 1, p. 51, 2019.

[9] P. Pisu and G. Rizzoni, "A comparative study of supervisory control strategies for hybrid electric vehicles," *IEEE Transactions on Control Systems Technology*, vol. 15, no. 3, pp. 506–518, 2007.

[10] H. Li, Y. Zhou, H. Xiong, B. Fu, and Z. Huang, "Real-time control strategy for CVT-based hybrid electric vehicles considering drivability constraints," *Applied Sciences*, vol. 9, no. 10, p. 2074, 2019.

[11] H. Borhan, A. Vahidi, A. M. Phillips et al., "MPC-based energy management of a power-split hybrid electric vehicle," *IEEE Transactions on Control Systems Technology*, vol. 20, no. 3, pp. 593–603, 2011.

[12] L. Johannesson, M. Asbogard, and B. Egardt, "Assessing the potential of predictive control for hybrid vehicle powertrains using stochastic dynamic programming," *IEEE Transactions on Intelligent Transportation Systems*, vol. 8, no. 1, pp. 71–83, 2007.

[13] W. Shabbir and S. A. Evangelou, "Real-time control strategy to maximize hybrid electric vehicle powertrain efficiency," *Applied Energy*, vol. 135, pp. 512–522, 2014.

[14] N. Kim, S. Cha, and H. Peng, "Optimal control of hybrid electric vehicles based on Pontryagin's minimum principle," *IEEE Transactions on Control Systems Technology*, vol. 19, no. 5, pp. 1279–1287, 2010.

[15] T. Katrašnik, "Analytical framework for analyzing the energy conversion efficiency of different hybrid electric vehicle topologies," *Energy Conversion and Management*, vol. 50, no. 8, pp. 1924–1938, 2009.

[16] T. Katrasnik, F. Trenc, and S. R. Opresnik, "Analysis of energy conversion efficiency in parallel and series hybrid powertrains," *IEEE Transactions on Vehicular Technology*, vol. 56, no. 6, pp. 3649–3659, 2007.

[17] T. Ott, F. Zurbriggen, C. Onder, and L. Guzzella, "Cycle-averaged efficiency of hybrid electric vehicles," *Proceedings of the Institution of Mechanical Engineers, Part D: Journal of Automobile Engineering*, vol. 227, no. 1, pp. 78–86, 2013.

[18] X. Hu, N. Murgovski, L. Johannesson, and B. Egardt, "Energy efficiency analysis of a series plug-in hybrid electric bus with different energy management strategies and battery sizes," *Applied Energy*, vol. 111, pp. 1001–1009, 2013.

[19] N. J. Schouten, M. A. Salman, and N. A. Kheir, "Energy management strategies for parallel hybrid vehicles using fuzzy logic," *Control Engineering Practice*, vol. 11, no. 2, pp. 171–177, 2003.

[20] H. Yang, S. Cho, N. Kim et al., "Analysis of planetary gear hybrid powertrain system part 1: input split system," *International Journal of Automotive Technology*, vol. 8, no. 6, pp. 771–780, 2007.

[21] H. Yang, B. Kim, Y. Park, W. Lim, and S. Cha, "Analysis of planetary gear hybrid powertrain system part 2: output split system," *International Journal of Automotive Technology*, vol. 10, no. 3, pp. 381–390, 2009.

[22] C. F. Yin, S. H. Wang, C. Q. Yu et al., "Fuzzy optimization of energy management for power split hybrid electric vehicle based on particle swarm optimization algorithm," *Advances in Mechanical Engineering*, vol. 11, no. 2, Article ID 1687814019830797, 2019.

[23] Q. N. Wang, W. Wang, P. Y. Wang et al., "Determination of the best seperation factor for power-split hybrid electric vehicle based on instantaneous efficiency," *Journal of Jilin University (Engineering and Technology Edition)*, vol. 43, no. 5, pp. 1160–1164, 2013, in Chinese.

[24] F. Zhu, L. Chen, and C. Yin, "Design and analysis of a novel multimode transmission for a HEV using a single electric machine," *IEEE Transactions on Vehicular Technology*, vol. 62, no. 3, pp. 1097–1110, 2013.

[25] I. Kim and H. Kim, "Configuration analysis of plug-in hybrid systems using global optimization," *World Electric Vehicle Journal*, vol. 6, no. 2, pp. 391–404, 2013.

[26] A. Szumanowski and Y. Yuhua Chang, "Battery management system based on battery nonlinear dynamics modeling," *IEEE Transactions on Vehicular Technology*, vol. 57, no. 3, pp. 1425–1432, 2008.

[27] V. Sezer, M. Gokasan, and S. Bogosyan, "A novel ECMS and combined cost map approach for high-efficiency series hybrid electric vehicles," *IEEE Transactions on Vehicular Technology*, vol. 60, no. 8, pp. 3557–3570, 2011.

[28] D. Shi, S. Wang, Y. Cai, and L. Chen, "Stochastic predictive energy management of power split hybrid electric bus for real-world driving cycles," *IEEE Access*, vol. 6, pp. 61700–61713, 2018.

[29] B. Škugor, J. Deur, M. Cipek, and D. Pavković, "Design of a power-split hybrid electric vehicle control system utilizing a rule-based controller and an equivalent consumption minimization strategy," *Proceedings of the Institution of Mechanical Engineers, Part D: Journal of Automobile Engineering*, vol. 228, no. 6, pp. 631–648, 2014.

[30] M. Cipek, D. Pavković, and J. Petrić, "A control-oriented simulation model of a power-split hybrid electric vehicle," *Applied Energy*, vol. 101, pp. 121–133, 2013.